Broadband pump-probe spectroscopy at 20-MHz modulation frequency

FABRIZIO PREDA, VIKAS KUMAR, FRANCESCO CRISAFI, DIANA GISELL FIGUEROA DEL VALLE, GIULIO CERULLO AND DARIO POLLI*

CNR-IFN and Dipartimento di Fisica, Politecnico di Milano, Piazza L. da Vinci 32, 20133 Milano (Italy)
**Corresponding author: dario.polli@polimi.it*

Received 28 April 2016; revised 24 May 2016; accepted 25 May 2016; posted 25 May 2016 (Doc. ID 263685); published 23 June 2016

We introduce an innovative high-sensitivity broadband pump-probe spectroscopy system, based on Fourier-transform detection, operating at 20-MHz modulation frequency. A common-mode interferometer employing birefringent wedges creates two phase-locked delayed replicas of the broadband probe pulse, interfering at a single photodetector. A single-channel lock-in amplifier demodulates the interferogram, whose Fourier transform provides the differential transmission spectrum. Our approach combines broad spectral coverage with high sensitivity, thanks to high-frequency modulation and detection. We demonstrate its performances by measuring two-dimensional differential transmission maps of a carbon nanotubes sample, simultaneously acquiring the signal over the entire 950-1350 nm range with $2.7\cdot10^{-6}$ rms noise over 1.5s integration time.

OCIS codes: *(300.6500) Spectroscopy, time-resolved; (300.6300) Spectroscopy, Fourier transforms; (300.6530) Spectroscopy, ultrafast; (120.6200) Spectrometers and spectroscopic instrumentation*

http://dx.doi.org/10.1364/OL.41.002970

Pump-probe is the most versatile and widely used ultrafast spectroscopy technique, which allows one to measure the excited-state dynamics of a great variety of samples [1]. In pump-probe an energetic pump pulse, resonant with a transition of the system under study, promotes population from the ground to the excited state; the subsequent system evolution is monitored by measuring the transmission change of a weak probe pulse, as a function of the pump-probe delay τ [2]. To gain the maximum information on the system dynamics, the signal should be detected for several transition energies; this is typically accomplished by using a broadband probe pulse and measuring the wavelength-(λ_{pr}) and delay-(τ) dependent differential transmission signal $\Delta T/T(\lambda_{pr},\tau)$. To this end, two approaches are possible: a serial one, which measures $\Delta T/T$ dynamics at individual probe wavelengths, and obtains the $\Delta T/T(\lambda_{pr},\tau)$ map by stacking the time traces together; a parallel one, which uses a spectrometer to separate the different frequency components of the probe pulse, which are then measured simultaneously by a multichannel detector. The parallel approach is preferable because it greatly reduces the measurement time, minimizing distortions in the retrieved spectra, due to slow drifts in the pump power, gradual sample damage or gradual misalignment of the detection chain or the spatial overlap of the two pulses.

$\Delta T/T$ signals in pump-probe are typically very small and lie on a large background, so that they require modulation transfer techniques for their measurement. These techniques consist in: (i) amplitude modulation of the pump through a mechanical chopper, an acousto-optic or an electro-optic modulator, ideally at a frequency exactly locked to half the repetition rate of the laser, so as to benefit from the enhanced energy correlation of consecutive laser pulses; (ii) synchronous demodulation of the probe to detect the pump-induced transmission changes. The sensitivity of pump-probe depends on the repetition rate of the system: it is $10^{-4}\div10^{-5}$ for high-pulse-energy amplified laser systems running at ~kHz repetition rate [2-11], and $10^{-6}\div10^{-7}$ for low-energy laser oscillators running at ~MHz repetition rate [12].

For kHz lasers parallel detection is straightforward to implement, using an optical multichannel analyzer (OMA), which consists in an imaging spectrometer that disperses the broadband probe beam onto a multi-channel line camera (either a CCD or an array of photodiodes) capable of single-shot detection at the full laser repetition rate [2-11]. The single-shot sensitivity of the detection chain (not considering the laser fluctuations) is typically limited to $\Delta T/T\sim10^{-3}$ per spectrum by an interplay of the electronic/read-out noise of the camera and the shot noise associated with the 10^5-10^6 electrons full-well capacity of the individual pixels. Using a camera running at 10-kHz readout frequency and a very stable laser source, Kukura *et al.* [10] demonstrated sensitivities down to $\Delta T/T<10^{-5}$ within 1-second measurement time. Analogously, Brixner *et al.* [11] presented a pump-probe scheme based on a fast camera with 100-kHz readout frequency, which provides single-shot sensitivity of $7.5\cdot10^{-3}$ in

absorbance change, limited by the laser intensity fluctuations, which translates into $\Delta T/T \sim 6 \cdot 10^{-5}$ within 1-second measurement time.

For MHz lasers no OMAs capable of single-shot detection exist, so that the serial approach is typically used, measuring $\Delta T/T$ dynamics at individual probe wavelengths, selected by an interference filter or a monochromator, using a photodiode connected to a high-frequency lock-in amplifier. Multi-channel lock-in amplifiers have been proposed but they are expensive, with limited channel number and/or repetition rate, and result in bulky and complicated setups [13, 14].

In this paper we introduce a new approach to broadband pump-probe spectroscopy, based on time-domain Fourier-transform (FT) detection and employing a single detector combined with a high-frequency modulator and lock-in amplifier. After the sample, the broadband probe pulse is sent to a linear interferometer that creates two collinear replicas with relative delay t. The two replicas interfere on the detector, giving rise to an interferogram, whose FT with respect to t is the spectrum of the unperturbed probe pulse [15]. Due to the linearity of the FT operator, the FT of the interferogram of the ΔT signal, as recorded by the lock-in, gives the ΔT spectrum. Our approach has the advantage of combining broad spectral coverage, thanks to the FT detection, and high sensitivity, thanks to the high frequency (up to 20 MHz, i.e. half the repetition rate of the laser) modulation and detection. Scanning the delay line only once per $\Delta T/T(\lambda_{pr}, \tau)$ map also speeds up the collection process with respect to the serial approach, as during movement the acquisition is blocked.

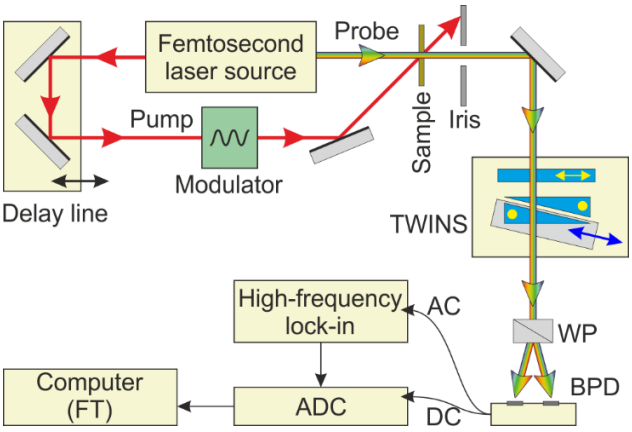

Fig. 1. Schematic drawing of the setup. WP: Wollaston prism; BPD: balanced photodiode; ADC: analog-to-digital conversion board. The directions of the optical axis of the birefringent materials in TWINS are indicated in yellow. The blue and black arrows indicate the direction of movement of translating stages.

A conceptual scheme of the experimental setup is shown in Fig. 1. A femtosecond laser source provides both the pump beam, resonant with the sample absorption, and the broadband probe beam, covering the spectral bandwidth of interest. The pump is sent to a motorized translation stage for delay control (M-405.CG from Physik Instrumente) and to an amplitude modulator for synchronous detection. Pump and probe beams are focused on the sample in a non-collinear geometry. After the sample, the probe light is selected by an iris and sent to a birefringent interferometer, which is a simplified version [16] of the Translating-Wedge-based Identical pulses eNcoding System (TWINS), previously introduced by some of the authors [17]. It consists of two birefringent wedges and a birefringent plate, with perpendicular orientation of their optical axes (as indicated in yellow in Fig. 1); the incoming pulse, polarized at 45° with respect to the directions of the optical axes, is split into two delayed pulses with perpendicular polarization. A polarizer before the TWINS can be inserted to control the polarization of the probe beam in case of depolarization induced by the sample birefringence or other spurious effects. This configuration is equivalent to a Babinet-Soleil compensator, with the difference that, while the Babinet-Soleil compensator is typically used as a variable waveplate, generating a retardation of one or a few cycles, TWINS is designed to provide retardation of hundreds of optical cycles, thus working as a pulse pair generator. Thanks to the inherent phase stability of the common-mode TWINS interferometer, the two delayed replicas are phase-locked with stability better than $\lambda/100$, enabling us to measure interferograms with an extremely high accuracy. The delay between the two replicas can be easily controlled by moving one wedge with a motorized translation stage (LMS-60 from Physik Instrumente). The direction of movement (see blue arrow in Fig. 1) is chosen to keep constant the distance of the two wedges, thus avoiding any displacement of the output beam. We measured only during the forward movement of the wedge, which was then sent back to its starting position at high speed (~60 mm/s) in parallel with the movement of the pump-probe delay stage. The optical axis of the fixed birefringent plate is perpendicular with respect to the one of the wedges, so that it reverts the relative delays of the two replicas. Moreover, its thickness is intermediate between the total thickness of the two wedges at maximum and minimum insertion, thus enabling us to scan across zero relative delay and record symmetric interferograms.

After the TWINS, a Wollaston prism (WP10 from Thorlabs) oriented at 45° with respect to the optical axis of the wedges separates the probe into two orthogonally polarized beams, each containing an interferogram (generated by the interference between the two pulse replicas) but with a relative phase shift of π. The two generated beams are eventually measured with the photodiodes of a balanced detector (Thorlabs PDB450A for the visible and PDB450C for the infrared). Since the balanced output of the detector is the difference between the two input channels, the common-mode signal is cancelled out, resulting in an interferogram with doubled amplitude and zero offset. Alternatively, one can replace the Wollaston prism with a polarizer oriented at 45° and use a single-channel photodiode, thus simplifying the experimental configuration at the cost of reducing the amplitude of the measured interferogram. The AC output of the balanced photodiode is sent to a high-frequency lock-in amplifier (HF2LI from Zurich Instruments). An analog-to-digital conversion card simultaneously records the demodulated signal from the lock-in and the DC output of the photodiode (as illustrated in Fig. 1) as a function of the wedge position x_w. These two waveforms are called the differential interferogram $\Delta T(x_w)$ and the linear probe interferogram $T(x_w)$, respectively. We first apply a super-Gaussian apodization window, to remove spectral side lobes caused by the finite sampled temporal interval, and then we compute their FTs, thus obtaining the differential transmission spectrum $\Delta T(\lambda_{pr}, \tau)$ and the linear transmission spectrum $T(\lambda_{pr})$ of the sample. A proper calibration is required to retrieve the wavelength axis from the FT frequency axis. To this purpose one can perform an interpolation, that will not cross the origin due to the partially rotating frame [17], using a series of

interference filters or a sample with a structured transmission spectrum [16]. The main advantage of this procedure is that, thanks to the linearity of the FT operator, to retrieve the $\Delta T(\lambda_{pr}, \tau)$ spectrum we do not need to record two interferograms of the perturbed and unperturbed sample and compute the difference of their FTs, but we can just record the interferogram of the ΔT signal, measured by the lock-in, and compute its FT. This approach was already demonstrated for broadband stimulated Raman scattering (SRS) microscopy [18]. By repeating this procedure at different delays, one can then build the two-dimensional $\Delta T/T(\lambda_{pr},\tau)$ map.

Particular attention must be paid to the phasing of the interferograms. Slight shifts of the zero-delay position would indeed cause serious errors in the retrieved spectral line shapes. By definition, interferograms should be symmetric functions, but experimental errors – such as electronic noise, laser fluctuations, misalignments of the detection chain or irregularities in the moving parts – can introduce asymmetries. Moreover, the lock-in amplifier is a signal integrator with finite response time, depending on the selected time constant. We typically set it to a value ~100 times smaller than the time required for the wedge to scan a fringe of the interferogram, of the order of 100 µs. Nonetheless, the differential interferogram $\Delta T(x_w)$ is still affected by a non-negligible delay with respect to the linear probe interferogram $T(x_w)$, because the latter directly comes from the photodiode with no delay. Therefore, we took special care in: (i) designing a proper phasing algorithm that finds the peak of the self-convolution of an interferogram to flatten its FT phase around zero or π; (ii) calibrating the delay introduced by the lock-in amplifier and numerically compensating for it. The latter procedure is performed only once around zero pump-probe delay (where the ΔT signal is highest) accurately measuring the difference of the zero-delay positions (estimated by the phasing algorithm (i)) between the linear and differential interferogram, which is then kept fixed for the other pump-probe delays. We note that this procedure is not necessary in SRS spectroscopy, for which, in contrast to pump-probe, the signal does not change in sign, so that one can plot the modulus of the FT (that does not depend on the phasing of the interferogram) instead of its real part [18].

The spectral resolution of the retrieved signal is $\Delta\nu=1/t_{max}$, where t_{max} is the maximum delay between the two replicas. This delay is given by $t_{max}=GVM\cdot d$, where $GVM=(1/v_{ge}-1/v_{go})$ is the group velocity mismatch, v_{go} and v_{ge} are the group velocities for the ordinary and extraordinary polarizations, respectively, and d is the thickness of the birefringent material [17]. To improve the spectral resolution one can act either on the birefringent material, which affects the GVM for the specific wavelengths of interest, or on the apex angle α and travel range L of the moving wedge, which determine the maximum thickness $d = L\tan\alpha$ (in the hypothesis that the beam size is much smaller than L). We employed alpha-barium borate (α-BBO) wedges with apex angle α=7° and 25-mm lateral size, that can guarantee a spectral resolution at 1.1 µm down to ~5-nm.

We first benchmarked our setup against a standard OMA-based pump-probe spectrometer for a low repetition-rate laser. To this purpose, we measured $\Delta T/T$ spectra of a β-carotene sample in quinoline solution using an amplified Ti:Sapphire laser (Libra from Coherent Inc), generating 100-fs, 800-nm pulses at 2-kHz repetition rate. The pump pulse was the second harmonic of the laser at 400nm, modulated at 1-kHz frequency (synchronized with the laser clock) by a mechanical chopper, while the probe was a white-light supercontinuum generated in a 2-mm sapphire plate. Figure 2 plots as black squares the $\Delta T/T$ spectrum, at 1-ps pump-probe delay, measured using a standard OMA detection scheme [3] and as a red solid line the $\Delta T/T$ spectrum collected with our TWINS-based FT spectrometer under the same experimental conditions. The agreement is excellent, thus demonstrating the reliability of our new detection system for broadband pump-probe spectroscopy. We observe the well-known transient absorption signals of β-carotene [19]: photo-bleaching ($\Delta T/T>0$) of the transition from the ground-state to the first optically allowed S_2 state for wavelengths shorter than 525nm, and photo-induced absorption ($\Delta T/T<0$) from the dark S_1 state to a higher-lying S_n state, peaking at ~590 nm wavelength.

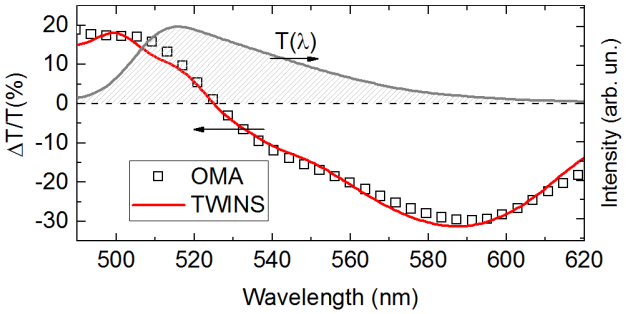

Fig. 2. Comparison of $\Delta T/T$ spectra collected on a β-carotene sample in solution at the same 1-ps delay using a standard OMA based on a CCD camera (squares) and the FT procedure here introduced (solid red line). Hashed area: probe spectrum.

We then applied our approach to a high-repetition rate laser system, for which no single-shot multi-channel detectors are available. We employed an Erbium-fiber oscillator (FemtoFiber Pro from Toptica Photonics), providing 70-fs pulses at 1.55-µm central wavelength and 40-MHz repetition rate. The output beam is divided into two branches, each amplified to 350-mW average power by two independent Er:doped fiber amplifiers (EDFAs). The output of the first EDFA is sent to a 2-mm-thick beta-barium borate (BBO) crystal, generating the pump pulse at the second harmonic (λ=780 nm). The pump beam is then sent to an acousto-optic modulator working at 20-MHz frequency (synchronized with the laser clock). The output of the second EDFA feeds a highly non-linear fiber, which broadens the spectrum of the incoming beam, producing a broadband (λ=940-1400 nm) probe beam (see gray hashed area in Fig. 3(c)).

We measured $\Delta T/T$ dynamics on a spin-coated sample of semiconducting single-walled carbon nanotubes (SWNTs) starting from a highly concentrated dispersion in orthodichlorobenzene [20]. The resulting sample presents a large number of bundles and aggregates, with a predominance of the (6,5) and the (7,5) chiralities, resulting in a broad absorption band of the first excitonic transition (S_{11}) centered at 1060 nm. Since no sharp spectral features are expected in the $\Delta T/T$ spectra, we aimed at a coarse spectral resolution of 50 nm, in order to maximize the recording speed. Therefore, we limited the TWINS travel range to L=3 mm, resulting in t_{max}=±75 fs maximum delay of the replicas. The wedge was translated at 6 mm/s constant speed, thus resulting in ~0.5 s measurement time for each $\Delta T/T$ spectrum. Increasing the scan range to L=15 mm it would also be possible to achieve 10-nm spectral resolution at the cost of increasing the measurement time to 2.5-s per spectrum. Representative linear $T(x_w)$ and differential

$\Delta T(x_w)$ interferograms at τ=100 fs delay are reported in Fig. 3(a), together with the apodization window used.

In Fig. 3(b) we plot the two-dimensional $\Delta T/T$ (λ_{pr}, τ) map, resulting from the average of three time scans. $\Delta T/T$ spectra at selected delays (100 fs, 1 ps and 3.5 ps) are plotted in Fig. 3(c) as solid lines. After photoexcitation, we see a strong positive signal, peaking at λ=1065 nm, due to ground-state photo-bleaching of the first excitonic transition of the SWNTs, which decays on the ps-timescale due to non-radiative ground-state recovery [21], with no significant change in the spectral profile. To highlight the population dynamics in the SWNT sample, we report as solid lines in Fig. 3(d) $\Delta T/T$ time traces at the peak of the signal (λ=1065 nm, red) and on its red-shifted shoulder (λ=1215 nm, black). Circles in Fig. 3(d) are fits to the data, using a simple sequential three-level rate-equation model to the single dynamics, typical of SWNTs, convoluted with the ~500-fs instrumental response function. The results indicate that excited-state population decays with a fast (150-180 fs) and a slow (1-3 ps, depending on the wavelength) time constant, in accordance with previous literature [22].

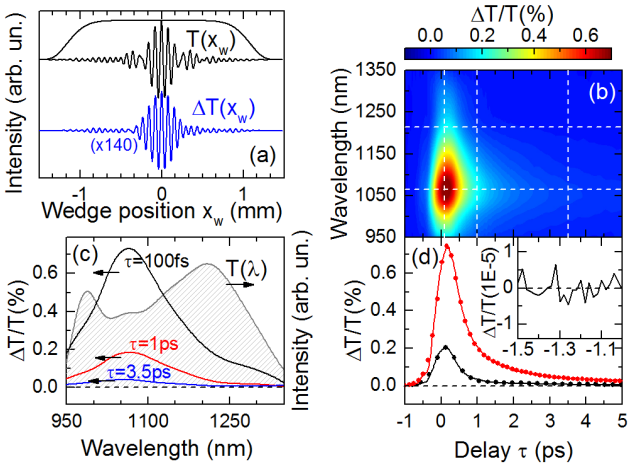

Fig. 3. (a) Apodized linear (black line) and differential (blue line) interferograms at 100fs delay, together with the apodization window used. (b) Two-dimensional $\Delta T/T(\lambda_{pr}, \tau)$ map for a SWNT sample. (c) Solid lines: $\Delta T/T$ spectra at selected probe delays as indicated; hashed area: probe spectrum. (d) $\Delta T/T$ dynamics (solid lines) and corresponding fits (circles) at selected probe wavelengths (red: λ=1065 nm; black: λ=1215 nm). Inset: close-up of the signal at λ=1215 nm for negative delays.

The real advantage of our detection scheme consists in running at high modulation frequencies, where the laser relative intensity noise is typically the lowest. This is clear by taking a closer look at the dynamics at λ=1215 nm (i.e. at to the peak of the probe spectrum) and negative delays (see inset of Fig. 3(d)). The peak-to-peak fluctuations of the signal around zero (with our 1.5-s integration time per delay) are of the order of $\pm 5\times10^{-6}$, and the corresponding rms noise is as low as 2.7×10^{-6}. It should be emphasized that, like several other fiber-based lasers, our system is not shot-noise limited, even at high frequencies [23], but has significant excess noise; using a more stable laser would hence enable us to reduce the rms noise even further.

In conclusion, we have proposed and experimentally demonstrated an innovative detection scheme for pump-probe spectroscopy, which combines a broad spectral coverage with very high modulation frequencies. This enables us to perform broadband measurements with an excellent signal-to-noise ratio in a short time. Our scheme, based on a single detector and lock-in amplifier, is significantly less expensive and complex than other implementations using a high-frequency multi-channel lock-in, which could in principle provide even higher sensitivity. This apparatus relies on the stability of the TWINS interferometer, whose common-path geometry allows one to control the delay between two pulses with a precision of attoseconds, without any active control or feedback. Thanks to this feature, the technique here proposed can be straightforwardly extended also to other spectral regions, from the UV to the mid-IR.

Funding. We acknowledge support by the European Research Council Consolidator Grant VIBRA (ERC-2014-CoG No. 648615), Advanced Grant STRATUS (ERC-2011-AdG No. 291198) and Proof of Concept Grant MISSION (ERC-2014-POC No. 665635).

References

1. S. Mukamel, *Principles of Nonlinear Optical Spectroscopy* (Oxford University Press, USA, 1995).
2. U. Megerle, I. Pugliesi, C. Schriever, C. F. Sailer, E. Riedle, Appl. Phys. B **96**, 215 (2009).
3. D. Polli, L. Lüer, and G. Cerullo, Rev. Sci. Instrum. **78**, 103108 (2007).
4. A. L. Dobryakov, S. A. Kovalenko, A. Weigel, J. L. Pérez-Lustres, J. Lange, A. Müller, and N. P. Ernsting, Rev. Sci. Instrum. **81**, 113106 (2010).
5. M. Bradler and E. Riedle, J. Opt. Soc. Am. B **31**, 1465 (2014).
6. A. Wand, R. Rozin, T. Eliash, K.-H. Jung, M. Sheves, and S. Ruhman, J. Am. Chem. Soc. **133**, 20922 (2011).
7. A. Maciejewski, R. Naskrecki, M. Lorenc, M. Ziolek, J. Karolczak, J. Kubicki, M. Matysiak, and M. Szymanski, Journal of Molecular Structure **555**, 1 (2000).
8. M. Raytchev, E. Pandurski, I. Buchvarov, C. Modrakowski, and T. Fiebig, J. Phys. Chem. A **107**, 4592 (2003).
9. S. Bourquin, R. P. Prasankumar, F. X. Kärtner, J. G. Fujimoto, T. Lasser, and R. P. Salathé, Opt. Lett. **28**, 1588 (2003).
10. F. M. Liebel, C. Schnedermann, T. Wende, and P. Kukura, J. Phys. Chem., **119**, 9506 (2015).
11. F. Kanal, S. Keiber, R. Eck, and T. Brixner, Opt. Expr. **22**, 16965 (2014).
12. H. Baida, D. Mongin, D. Christofilos, G. Bachelier, A. Crut, P. Maioli, N. Del Fatti, and F. Vallée, Phys. Rev. Lett. **107**, 057402 (2011).
13. C.-W. Luo, Y.-T. Wang, A. Yabushita, and T. Kobayashi, Optica **3**, 82 (2016).
14. N. Ishii, E. Tokunaga, S. Adachi, T. Kimura, H. Matsuda, and T. Kobayashi, Phys. Rev. A **70**, 023811 (2004).
15. B. C. Smith, *Fundamentals of Fourier Transform Infrared Spectroscopy* (CRC Press, 2011).
16. A. Oriana, J. Réhault, F. Preda, D. Polli, and G. Cerullo, J. Opt. Soc. A, submitted (2016).
17. D. Brida, C. Manzoni, and G. Cerullo, Opt. Lett. **37**, 3027 (2012).
18. J. Réhault, F. Crisafi, V. Kumar, G. Ciardi, M. Marangoni, G. Cerullo, and D. Polli, Opt. Expr. **23**, 25235 (2015).
19. T. Polívka, and V. Sundström, Chem. Rev. **104**, 2021 (2004).
20. L. N. Glanzmann, D. J. Mowbray, D. G. Figueroa del Valle, F. Scotognella, G. Lanzani, and A. Rubio, J. Phys. Chem. C **120**, 1926 (2016).
21. J.-S. Lauret, C. Voisin, G. Cassabois, C. Delalande, Ph. Roussignol, O. Jost, and L. Capes, Phys. Rev. Lett. **90**, 057404 (2003).
22. L. Lüer, S. Hoseinkhani, D. Polli, J. Crochet, T. Hertel, and G. Lanzani, Nat. Phys. **5**, 54 (2009).
23. N. Coluccelli, V. Kumar, M. Cassinerio, G. Galzerano, M. Marangoni, and G. Cerullo, Opt. Lett. **39**, 3090 (2014).